JAERI-M
83-174

PHYSICS DESIGN CONSIDERATIONS OF STEADY AND QUASI-STEADY FUSION EXPERIMENTAL REACTOR BY LOWER HYBRID WAVE CURRENT DRIVE

October 1983

Masayoshi SUGIHARA, Noboru FUJISAWA,
Takumi YAMAMOTO, Tatsuhiro YOSHIZU*,
Akihiro NAKAJIMA*, Koju UEDA**, Satoshi NISHIO
and Hiromasa IIDA

日本原子力研究所
Japan Atomic Energy Research Institute

JAERI-Mレポートは，日本原子力研究所が不定期に公刊している研究報告書です。
入手の問合わせは，日本原子力研究所技術情報部情報資料課（〒319-11茨城県那珂郡東海村）あて，お申しこしください。なお，このほかに財団法人原子力弘済会資料センター（〒319-11 茨城県那珂郡東海村日本原子力研究所内）で複写による実費頒布をおこなっております。

JAERI-M reports are issued irregularly.
Inquiries about availability of the reports should be addressed to Information Section, Division of Technical Information, Japan Atomic Energy Research Institute, Tokai-mura, Naka-gun, Ibaraki-ken 319-11, Japan.

編集兼発行　日本原子力研究所
印　　刷　㈱高野高速印刷

JAERI-M 83-174

Physics Design Considerations of Steady and Quasi-Steady Fusion Experimental Reactor by Lower Hybrid Wave Current Drive

Masayoshi SUGIHARA, Noboru FUJISAWA, Takumi YAMAMOTO[+]
Tatsuhiro YOSHIZU[*], Akihiro NAKAJIMA[*], Koju UEDA[**]
Satoshi NISHIO and Hiromasa IIDA

Department of Large Tokamak Development,
Tokai Research Establishment, JAERI

(Received October 4, 1983)

Optimum plasma and rf parameters for possible scenarios of fusion experimental reactor (FER) by lower hybrid wave current drive are studied by simple physical model equations. Two scenarios are considered: I) quasi-steady, II) steady operation. In scenario I, the minimization of the recharge time of OH coils or stored energy for it is essential and can be realized by driving sufficient current without increasing the plasma temperature too much. Low plasma density and broad wave spectrum are shown to be favorable for the minimization. In the case of FER baseline parameter, the minimum recharge time is 3∿5 sec/Volt·sec. In scenario II, the energy multiplication factor Q is essential and can be maximized by appropriately adjusting the plasma density, temperature and wave spectrum, under the restriction of the accessibility condition, safety factor at the plasma surface, beta poloidal and toroidal limitations. Fairly narrow wave spectrum is needed and the maximum attainable Q value for various energy confinement scalings and various major radii is 5∿10.

Keywords: Tokamak, Fusion Experimental Reactor, Physics Design, Current Drive, Lower Hybrid Wave, Steady Operation, Duty Cycle

---

+ Department of Thermonuclear Fusion Research, Tokai, JAERI

* Keio University, Hiyoshi, Yokohama.

** Mitsubishi Electric Co. Ltd., Tokyo

JAERI−M 83−174

低域混成波を用いた電流駆動による定常および準定常核融合実験炉の物理設計

日本原子力研究所東海研究所大型トカマク開発部
杉原　正芳・藤沢　　登・山本　　巧[+]・吉津　達弘[*]
中島　昭裕[*]・上田　孝寿[**]・西尾　　敏・飯田　浩正

（１９８３年１０月４日受理）

低域混成波を用いた電流駆動による，核融合実験炉の可能なシナリオに対する最適なプラズマおよび高周波波動のパラメータを簡単な物理モデル方程式によって検討した。検討は，(I) 準定常，(II) 定常，の二つのシナリオについて行った。シナリオⅠにおいては，変流器コイルの反転時間の最小化又はそのために必要な蓄積エネルギーの最小化が重要であり，それはプラズマ温度を余り高くせずに十分に大きな高周波駆動電流を流すことによって達成できる。低密度で巾の広い波のスペクトルがこのために必要であることが示された。核融合実験炉の基本パラメータに対しては，最小反転時間は３～５秒／磁束である。シナリオⅡにおいては，エネルギー増倍率Qが重要であり，波の近接性，トロイダルおよびポロイダルベータ値，プラズマ表面の安全係数等の制約のもとでプラズマ密度，温度および波のスペクトルを適当に選ぶことによって最大とすることができる。かなり狭い波のスペクトルが要求され，最大のQ値は，いろいろなエネルギー閉じ込め時間や装置の大半径に対して５～１０が得られた。

＋　核融合研究部
＊　慶応義塾大学理工学部
＊＊　三菱電機（株）

Contents

1. Introduction 1
2. Basic Model Equations 3
3. Results 12
1. Optimum plasma and rf parameters for Scenario I 12
2. Optimum plasma and rf parameters for Scenario II 16
4. Conclusions 21
References 23

目　　次

1. 序　論 1
2. 基礎モデル方程式 3
3. 計算結果 12
1. シナリオⅠの最適プラズマおよび高周波パラメータ 12
2. シナリオⅡの最適プラズマおよび高周波パラメータ 16
4. 結　論 21
参 考 文 献 23

1. Introduction

It has been clarified by the design study of FER (Fusion Experimental Reactor) [1, 2] and INTOR [3∿5] that the steady operation will mitigate the engineering difficulties in a tokamak fusion reactor to a great degree. To realize the steady operation in a tokamak reactor, some method of non-inductive current drive must be employed. Recently, current drive by the lower hybrid range of frequency wave (LHW) has been proposed theoretically [6, 7] and demonstrated experimentally [8∿11]. Design studies of the steady tokamak reactors by LHW have also been done [12, 13]. A schematic drawing of this operation scenario (Scenario Ⅱ) is shown in Fig. 1. Experimentally, however, almost all of the current drive experiments have been restricted to low density discharges (order of 10^{18} m^{-3}) [8∿11]. If this restriction is true even for future reactor, steady operation with high Q (energy multiplication factor) value can never be expected.

Quasi-steady operation may be a promissing scenario under this restriction. A schematic drawing of this operation scenario (Scenario I) is shown in Fig. 2. In this scenario, the plasma current in the burning phase is sustained by usual OH coils. When the burning phase is terminated, the plasma density is lowered and the plasma current is kept constant by the lower hybrid wave current drive during the recharging of OH coils. In this way, the plasma current is kept almost constant over the entrie phase. Since almost all of the flux by OH coils can be used to sustain the plasma current in the burning phase with high electron temperature, the burn time can be prolonged by an order of magnitude. Possible advantages for the reacotr engineering by the scenario I and Ⅱ are summarized in Table 1.

In the present paper, we choose Scenario I and II as typical possible scenarios for quasi-steady and steady tokamak reactor driven by LHW, and investigate the optimum plasma and rf parameters for both scenarios on the basis of the quasi-linear theory of the current drive.

In Scenraio II, we assume that the density restriction in today's experiments is removed. Thus, it should be noted that Scenario I will be based on a more certain data base, while Scenario II is less certain. Since rf power for current drive concurrently heats the plasma, rf current drive is strongly coupled with the power balance of the plasma. Thus, driven current and deposited rf power must be obtained consistently with the power balance. In Scenario I, OH coil recharge time τ_r or required stored energy $\tau_r P_{rf}$ (P_{rf} is the required rf power for current drive) will be an essential parameter for optimization. We will obtain the plasma and rf parameters for minimizing τ_r or $\tau_r P_{rf}$. In Scenario II, Q value will be an essential parameter, so that we will obtain an optimum plasma and rf parameters for maximizing Q value under the restriction of the accessibility condition.

Although it is rather difficult to treat the detailed physical process of the waves in plasmas by a simple physical model, it is very important to develop such a model for the conceptual design study. This is our primary concern of the present paper. Thus, emphases of the study are placed on the rough evaluation of the plasma and rf parameters for the conceptual design study of steady or quasi-steady reactor. Our primary interest is the feasibility and possible problems of both scenarios, so that more detailed calculations such as ray-tracing including the toroidal effect, reflection at the wall are beyond the scope of this study. They will be our future study.

In §2, basic model equations are presented and a simple comparison

with the experiments is made. In §3, detailed parametric survey to obtain optimum plasma and rf parameters for Scenario I and II is carried out. Possible problems are also clarified. Conclusions are drawn in §4.

2. Basic Model Equations

Electron plasma current is driven by LHW via the process of the energy and momentum absorption by resonant electrons. According to the quasi-linear theory of the current drive by LHW, the driven current and the deposited power are determined by the balance of the quasi-linear flattening of the electron velocity distribution function and the collisional relaxation with the field particles to the equilibrium Maxwellian distribution [6, 7]. When the intensity of the wave spectrum is sufficiently large, the saturated driven current density $j_{rf}(r)$ and deposited power per unit volum $p_{rf}(r)$ are given as [12, 13]

$$j_{rf}(r) = 6.64 \times 10^{-9} \frac{n_e(r)}{\sqrt{T_e(r)}} \exp\left[-\frac{2.56 \times 10^5}{n_{z_1}^2 T_e(r)}\right] \left(\frac{1}{n_{z_2}^2} - \frac{1}{n_{z_1}^2}\right) \ (A/m^2), \quad (2.1)$$

$$p_{rf}(r) = 3.79 \times 10^{-29} K \frac{n_e^2(r)}{\sqrt{T_e(r)}} \exp\left[-\frac{2.56 \times 10^5}{n_{z_1}^2 T_e(r)}\right] \ell n \frac{n_{z_1}}{n_{z_2}} \ (W/m^3), \quad (2.2)$$

where $n_e(r)$, $T_e(r)$ are electron density and temperature at the position r. All units are MKS throughout the paper except for temperature (ev). n_{z_1} and n_{z_2} are the upper and lower refractive index of the wave in toroidal direction. Wave spectrum takes finite value between n_{z_1} and n_{z_2}, and is assumed to be zero elsewhere. K is a correction factor which is obtained from the two-dimensional simulation in a velocity space, and we take K = 0.392 [7]. Waves propagate from the plasma surface to the central region, and dissipate their energy to drive the current. If, at some

with the experiments is made. In §3, detailed parametric survey to obtain optimum plasma and rf parameters for Scenario I and II is carried out. Possible problems are also clarified. Conclusions are drawn in §4.

2. Basic Model Equations

Electron plasma current is driven by LHW via the process of the energy and momentum absorption by resonant electrons. According to the quasi-linear theory of the current drive by LHW, the driven current and the deposited power are determined by the balance of the quasi-linear flattening of the electron velocity distribution function and the collisional relaxation with the field particles to the equilibrium Maxwellian distribution [6, 7]. When the intensity of the wave spectrum is sufficiently large, the saturated driven current density $j_{rf}(r)$ and deposited power per unit volum $p_{rf}(r)$ are given as [12, 13]

$$j_{rf}(r) = 6.64 \times 10^{-9} \frac{n_e(r)}{\sqrt{T_e(r)}} \exp\left[-\frac{2.56 \times 10^5}{n_{z_1}^2 T_e(r)}\right] \left(\frac{1}{n_{z_2}^2} - \frac{1}{n_{z_1}^2}\right) \ (A/m^2), \quad (2.1)$$

$$p_{rf}(r) = 3.79 \times 10^{-29} K \frac{n_e^2(r)}{\sqrt{T_e(r)}} \exp\left[-\frac{2.56 \times 10^5}{n_{z_1}^2 T_e(r)}\right] \ell n \frac{n_{z_1}}{n_{z_2}} \ (W/m^3), \quad (2.2)$$

where $n_e(r)$, $T_e(r)$ are electron density and temperature at the position r. All units are MKS throughout the paper except for temperature (ev). n_{z_1} and n_{z_2} are the upper and lower refractive index of the wave in toroidal direction. Wave spectrum takes finite value between n_{z_1} and n_{z_2}, and is assumed to be zero elsewhere. K is a correction factor which is obtained from the two-dimensional simulation in a velocity space, and we take K = 0.392 [7]. Waves propagate from the plasma surface to the central region, and dissipate their energy to drive the current. If, at some

point before the center, the driven current is lesser than the saturated value given by Eq. (2.1), any power to drive the current in the inner region of this point is not remained, so that the current profile will become a hollow profile. Double tearing mode will be anticipated to grow under this hollow profile [14, 15]. The consequance of this instability may have the possibility to lead to a new kind of MHD equilibria [12]. However, this question cannot be answered at present, and we take the basic stand point in the present paper that the hollow current profile must be avoided to prevent the possible occurence of plasma disruption. Total driven current I_{rf} and deposited power P_{rf} are calculated as follows.

$$I_{rf} = 2\pi \int_0^a j_{rf}(r)\, r\, dr \quad , \tag{2.3}$$

$$P_{rf} = 4\pi^2 R \int_0^a P_{rf}(r)\, r\, dr \quad , \tag{2.4}$$

where a and R are the plasma minor and major radii, respectively.

In addition to the sufficient strength of the wave spectrum, the accessibility condition for the slow wave must be satisfied to assure the penetration of the waves to the plasma center. This condition is given for the refractive index n_z in toroidal direction as follows [13].

$$n_z > n_{LC} = \left(1 - \frac{\omega^2}{\Omega_e \Omega_i}\right)^{-\frac{1}{2}} \qquad \omega \leq \omega_c \quad , \tag{2.5}$$

$$n_z > n_{LC} = \frac{\omega_{pe}}{\Omega_e} + \left[1 + \left(\frac{\omega_{pe}}{\Omega_e}\right)^2 \left(1 - \frac{\Omega_e \Omega_i}{\omega^2}\right)\right]^{\frac{1}{2}} \quad \omega \geq \omega_c \quad , \tag{2.6}$$

where

$$\omega_c^2 \equiv \frac{\omega_{pe}^2 \Omega_i}{2\Omega_e} \left[\left(1 + \frac{4\Omega_e^2}{\omega_{pe}^2}\right)^{\frac{1}{2}} - 1\right] \quad . \tag{2.7}$$

Here, ω, ω_{pe}, Ω_e, Ω_i are frequency of LHW, electron plasma frequency, electron and ion cyclotron frequency, respectively. Usually, lower cutoff value of n_{LC} takes its maximum at the intermediate region of the plasma

column. We will choose this maximum value for n_{z2} in Eqs. (2.1) and (2.2) to ensure the sufficient penetration of the waves to the center. We will neglect the variation of n_{z1} and n_{z2} during the wave propagation for simplicity.

Most important restriction for the determination of the wave frequency comes from the condition to avoid the parametric instabilities. It has been shown that when the following condition

$$\omega \gtrsim 2\ \omega_{LH}(o) \tag{2.8}$$

is satisfied, the instabilities with the greatest growth rate can be avoided [16, 17]. Thus, we set ω to $2\omega_{LH}(o)$, where $\omega_{LH}(o)$ is the lower hybrid frequency at the plasma center.

Figure 3 shows the total driven current and the current drive efficiency I_{rf}/P_{rf} for various average electron density in the limit of the sufficiently strong intensity of the wave spectrum calculated by Eqs. (2.1), (2.2). Average electron temperature is assumed to be 1 keV and the following profiles for density and temperature are employed.

$$n_e(r) = n_0\ [1 - (\frac{r}{a})^4] + n_b \quad , \tag{2.9}$$

$$T_e(r) = n_0\ [1 - (\frac{r}{a})^2] + T_b \quad , \tag{2.10}$$

where n_0, n_b, T_0, T_b are central and boundary densities and temperatures. We assume $n_b = 1 \times 10^{16}$ m^{-3} and $T_b = 50$ eV. As a device parameter, we have used those of FER. They are tabulated in Table 2. We also assumed that $n_{z1} = c/3\bar{v}_e = 7.54$. n_{z2} takes its maximum at some point between the plasma surface and the center. We used this maximum value for n_{z2} to ensure the sufficient penetration. This value increases as the plasma density becomes high, resulting in narrower wave spectrum. Consequently, the driven

current deviates down from the linear dependence on $\bar{n}_e$ expected in Eq. (2.1). In Fig. 3, the current drive efficiency obtained in PLT experiments is denoted by open circles for the various cases of the phase difference $\Delta\phi$ between ajacent wave guide [9]. Although, in this experiment, the electron temperature and the spectrum width are not clearly identified, the efficiency by the simple numerical model of Eqs. (2.1) and (2.2) roughly agrees with the experiment within a factor of 2. We also extrapolate the results of JFT-2 experiments [8] to the equivalent plasma with the electron temperature of 1 keV and denote it by an open triangle in the figure. From these results, we conclude that the estimations of the driven current and the deposited power by Eqs. (2.1)$\sim$(2.4) are roughly consistent with the experiments.

Eqs. (2.1)$\sim$(2.4) are very simple, so that they provide us a useful tool for a rough and wide range of the parametric survey for the conceptual design study. However, they do not include the spectrum modification due to the Landan damping during its propagation to the plasma center. Thus, when we are concerned with the spectrum width and intensity required to ensure the use of Eqs. (2.1)$\sim$(2.4), we must solve the more detailed set of equations for the current drive and wave absorption. This set of equations calculate the quasi-linear modification of the electron velocity distribution function $F(v_z)$ and the absorption of the wave spectrum $\tilde{P}_{rf}(n_z, r)$ in a cylindrical geometry with concentric magnetic surface as follows.

$$\frac{\partial F}{\partial X} = - \frac{X(1 - \bar{E}\, X^2)}{1 + X^3\, \bar{D}_{rf}(\tilde{P}_{rf})}\, F \quad , \tag{2.11}$$

$$\frac{\partial\, \tilde{P}_{rf}}{\partial r} = - \, 4\, \pi^2\, R\, r\, P_{ab}(n_z, r) \quad , \tag{2.12}$$

where $X = v_z/v_e$. v_e and v_z are the thermal velocity and the velocity in toroidal field direction of electrons at the position of r. $\bar{D}_{rf}$ and $\bar{E}$ are the normalized diffusion coefficient in the velocity space and the dc electric field. $P_{ab}(n_z, r)$ is the absorbed wave power and is given as

$$P_{ab}(n_z, r) = - m_e v_z \bar{D}_{rf} \frac{\partial F}{\partial v_z} \quad , \tag{2.13}$$

where m_e is the electron's mass. By solving the simultaneous differential equations of Eqs. (2.9)∿(2.11), the driven current density can be obtained as

$$j_{rf}(r) = - e \int_{-\infty}^{\infty} v_z F \, d \, v_z \quad . \tag{2.14}$$

It should be noted that the results of Eqs. (2.11)∿(2.14) reduce exactly to those of Eqs. (2.1)∿(2.4) when the spectrum intensity is sufficiently large. While, a certain part or even whole part of the wave spectrum can be absorbed in the peripheral region of the plasma, so that the profile and the amount of the driven current can be significantly altered from those of Eqs. (2.1)∿(2.4) when the spectrum intensity is not sufficiently large. These problems are essential for the design of the wave guide and rf system. In the present paper, we assume that the spectrum intensity is sufficiently large throughout the plasma, so taht Eqs. (2.1)∿(2.4) are reasonable evaluation of the driven current and deposited rf power. Consistency of the assumed wave spectrum intensity and width with the design of wave guide and rf system will be our future study.

Wave energy absorbed by the resonant electrons, whose velocity is usually relatively high, largely goes into the bulk electrons and thereby heat them through collisional relaxation process [6]. On the other hand, as seen from Eqs. (2.1), (2.2) the driven current and deposited power

strongly depend on the electron temperature. Therefore, it is essential to consider the plasma power balance consistently with the power deposition to the electron by the rf current drive. In the present paper, we will use the following simplified point model power balance equations for the average electron and ion temperatures $\bar{T}_e$ and $\bar{T}_i$,

$$G_e P_\alpha + P_R + P_J - P_{\chi e} - P_{sy} - P_{br} - P_{ei} - P_{imp} = 0 \quad , \tag{2.15}$$

$$(1 - G_e)P_\alpha + P_{ei} - P_{\chi i} = 0 \quad . \tag{2.16}$$

Here G_e is the fraction of α-particle energy transfered to the electrons, and we use the following simple expression [18]

$$G_e = (1 - \bar{T}_e/1.5\times 10^5)^2 \quad . \tag{2.17}$$

P_α, P_R, P_J, $P_{\chi e}$, $P_{\chi i}$, P_{sy}, P_{br}, P_{ei} and P_{imp} are α-particle heating, deposited power by current drive, joule heating by OH current, electron and ion transport energy loss, synchrotron radiation loss, bremsstrahlung radiation loss, electron-ion energy relaxation loss and radiation loss by impurities per unit volume, respectively, the expressions of which are presented as follows.

$$P_\alpha = \frac{1}{4}\bar{n}_i^2 \langle\sigma v\rangle E_\alpha f_\alpha \quad , \tag{2.18}$$

$$P_J = \eta j_{OH}^2 \quad , \tag{2.19}$$

$$P_{\chi e} = \frac{1.5\,\bar{n}_e\,\bar{T}_e}{\tau_{Ee}} \quad , \tag{2.20}$$

$$P_{\chi i} = \frac{1.5\,\bar{n}_i\,(1+f_z)\bar{T}_i}{\tau_{Ei}} \quad , \tag{2.21}$$

$$P_{sy} = 6.38\times 10^{-16}\, B^{2.5}\,\bar{T}_e^2\,\left(\frac{\bar{n}_e}{aA}\right)^{1/2} \quad , \tag{2.22}$$

$$P_{br} = 1.41 \times 10^{-38} Z_{eff} \bar{n}_e^2 \sqrt{\bar{T}_e} \quad , \tag{2.23}$$

$$P_{ei} = \frac{1.5 \bar{n}_e (\bar{T}_e - \bar{T}_i)}{\tau_{ei}} \quad , \tag{2.24}$$

where $\bar{n}_i$ and $\bar{n}_e$ are the average fuel ion and electron density. As for the energy confinement times τ_{Ee} and τ_{Ei}, we use Alcator and neoclassical scalings, which can reproduce the present-day experimental results. They are given as [19, 20]

$$\tau_{Ee} = 1.1 \times 10^{-20} \bar{n}_e a^2 \quad , \tag{2.25}$$

$$\tau_{Ei} = 4.7 \times 10^{18} \frac{B^2 \sqrt{\bar{T}_i} a^2}{A^{1.5} \bar{n}_i q_\psi^2} \quad , \tag{2.26}$$

where A, B and q_ψ are the aspect ratio, toroidal magnetic field on axis and the safety factor, respectively. The numerical coefficients of these expression may contain uncertainties, so that we introduce the ambiguity factor C_E and multiply Eqs. (2.25) and (2.26) by C_E. Possible cases with various values of C_E will be investigated. $\langle\sigma v\rangle$, E_α and f_α are the rate coefficient for D-T fusion reactions, the energy of α-particles and the correction factor representing the effect of the density and temperature profile on fusion power production, respectively. For the profiles of Eqs. (2.13) and (2.14), $f_\alpha \sim 1.5$ at $\bar{T} = 10$ keV. f_z is the ratio of the impurity ion density $\bar{n}_I$ to fuel ion density $\bar{n}_i$, $f_z = \bar{n}_I / n_i$. Effective charge of the plasma Z_{eff} is defined as

$$Z_{eff} = 1 + f_z Z^2 \quad , \tag{2.27}$$

where Z is the charge of the impurity. We assume oxygen impurity and calculate the radiation energy loss by using the coronal equilibrium model, for simplicity. By numerical fitting of the results of Ref. [21],

we obtain the expression for the radiation energy loss by oxygen impurities as

$$P_{imp} = f_z \cdot \bar{n}_e^2 \cdot 10^{0.679[\log_{10} \bar{T}_e/4 \times 10^3]^2 - 34} \quad (W/m^3) \quad . \qquad (2.28)$$

$$(2 \times 10^2 \text{ eV} \leq T_e \leq 10^4 \text{ eV})$$

τ_{ei} is the energy relaxation time between electrons and ions, and is given as

$$\tau_{ei} = 4.38 \times 10^{13} \frac{T_e^{3/2}}{\bar{n}_e} Z_{eff} \quad , \qquad (2.29)$$

where we have assumed that Coulomb logarithm is 18. η is the plasma resistivity for the joule current. We will use the classical one for η given as

$$\eta = 10^{-3} Z_{eff} \bar{T}_e^{-1.5} \quad (\Omega \cdot m) \quad , \qquad (2.30)$$

where we have neglected the effect of trapped electrons. It should be noted that j_{OH} consists of the current not only by the OH coils but also by the reverse electro-magnetic force generated by rf driven current.

To obtain the recharge time of OH coils, we will replace the tokamak system by the following equivalent circuit system;

$$\text{OH coil} : L_1 \frac{dI_1}{dt} + M_{12} \frac{dI_p}{dt} + M_{13} \frac{dI_3}{dt} = V_1 \quad , \qquad (2.31)$$

$$\text{Plasma} : M_{12} \frac{dI_1}{dt} + L_p \frac{dI_{OH}}{dt} + M_{23} \frac{dI_3}{dt} + (R_p + \frac{dL_p}{dt}) I_{OH}$$

$$= - L_p \frac{dI_{rf}}{dt} - \frac{dL_p}{dt} I_{rf} \quad , \qquad (2.32)$$

$$\text{Vertical coil} : M_{13} \frac{dI_1}{dt} + M_{23} \frac{dI_p}{dt} + L_3 \frac{dI_3}{dt} = V_3 \quad . \qquad (2.33)$$

Here, $I_p = I_{rf} + I_{OH}$ is the net plasma current, L and M are self and mutual inductance for each coils. We determine these circuit constants of the equivalent circuit for the actual poloidal coil configuration of FER, which provides the desired equilibrium configuration of the plasma. They are tabulated in Table 3, where we have assumed the number of turns of OH and vertical coils to be 200. V_1 and V_3 are the voltage of the power supply for each coil. R_p is the plasma resistance and is given as

$$R_p = \eta \frac{2R}{a^2 \kappa} \sim \frac{6.06 \times 10^{-3}}{\bar{T}_e^{3/2}} Z_{eff} \quad (\Omega) \quad . \tag{2.34}$$

The right hand side of Eq. (2.32) represents the reverse electro-magnetic force by rf current drive. We will assume, for simplicity, that $\dot{L}_p = 0$ and $I_p = 5.3$ MA = cost throughout the whole operation phase. Then, the recharge time τ_r for the flux of one volt·second, which links with the plasma, can be obtained from Eqs. (3.31), and (3.32) as

$$\tau_r = \frac{1}{R_p (I_{rf} - I_p)} \quad . \tag{2.35}$$

Then, when $\bar{T}_e$ is too large, τ_r becomes large due to the sharp decrease of R_p. When $\bar{T}_e$ is too small, again τ_r becomes too large or even negative due to the decrease of I_{rf}. Consequently, τ_r will take its minimum at some value of $\bar{T}_e$.

3. Resutls

1. Optimum plasma and rf parameters for Scenario I

The procedure to obtain the minimum recharge time τ_r and the minimum required stored energy $P_s \equiv \tau_r P_{rf}$ is as follows. First, we fix the electron density. Next, we solve the nonlinear simultaneous equations (2.15) and (2.16) for $\bar{T}_e$ and $\bar{T}_i$ with appropriately varying the wave refractive index n_{z1} and n_{z2}. In solving these equations, density and temperature profiles of Eqs. (2.13), (2.14) are assumed to calculate the driven current and deposited rf power. By using the obtained value of I_{rf}, which is consistent with the power balance through P_{rf}, τ_r and P_s are calculated from Eq. (2.35) with $I_p = 5.3$ MA. As can be seen from Eqs. (2.1) and (2.2), lower value of n_{z2} can drive current more effectively, that is, more current is driven by less rf power. Thus, the lowest value of n_{z2}, which satisfies the accessibility condition Eqs. (2.5)$\sim$(2.7), is preferable for the minimization of τ_r and P_s. Thus, the key parameter to minimize τ_r and P_s is the upper parallel refractive index n_{z1}. Figure 4 shows τ_r and P_s as a function of n_{z1} for $\bar{n}_e = 3 \times 10^{18}$ m^{-3} and no impurity contamination. When n_{z1} is small, $\bar{T}_e$ must be large to retain the number of resonant particles to a certain level (i.e. not to make the exponential term in Eq. (2.2) too small). Then R_p is small, so that τ_r is rather large. As n_{z1} becomes larger, $\bar{T}_e$ must become even smaller to satisfy the power balance, since the width of the resonance becomes wider. As a result, I_{rf} becomes smaller, while R_p becomes even larger so that τ_r becomes smaller. When n_{z1} becomes further large, the decrease of I_{rf} dominates the increase of R_p, so that τ_r again becomes large, even negative for too large n_{z1}. Consequently, τ_r and P_s take their minimum for some n_{z1} as shown in Fig. 4. Since $\bar{T}_e$ becomes smaller

as n_{z_1} becomes larger, P_{rf} becomes also smaller as n_{z_1}, so that $P_s \equiv \tau_r P_{rf}$ takes its minimum for larger n_{z_1} than τ_r. Fig. 5 shows the minimum value of τ_r as well as the recharge time, which makes P_s minimum, as a function of the average electron density. As is deduced from Eq. (2.35), larger R_p (smaller $\bar{T}_e$) makes τ_r smaller. This can be realized by larger efficiency of current drive. Thus, the minimum value of τ_r becomes smaller for smaller $\bar{n}_e$. Figures 6 and 7 show the driven current and deposited rf power, and average electron and ion temperatures for the minimum value of τ_r. Figure 8 shows the requried stored energy for the minimum values of τ_r and P_s. When we choose $\bar{n}_e = 3 \times 18^{18}$ m^{-3}, for example, and assume that the total volt·sec for OH coil is 100 V·s, the total requried stored energy is 2.4 GJ for Min(τ_r) and 1.7 GJ for Min(P_s). On the other hand, the total recharge time is 290 sec for Min(τ_r) and 340 sec for Min(P_s). There seems to be no significant difference bewteen the two cases. More elaborate and careful comparison of the cost-performance will be needed for the selection.

To decrease τ_r and P_s, lower density is preferable. When the density is too low, however, runaway discharge due to the large dc electric field from the OH coils might occur or some instability might be excited due to the large drift velocity of OH current. Figure 9 shows dc electric field E normalized by Dreicer electric field E_D and the electron drift velocity normalized by the electron thermal velocity as a function of $\bar{n}_e$ for Min(τ_r). As can be seen from this figure, dc electric field is sufficiently small compared with E_D unless $\bar{n}_e$ is too small. On the other hand, v_d/v_e is rather large compared with the conventional tokamak discharge ($\gtrsim 10^{-2}$). One possible instability, which might be excited, is a drift instability. Electron energy confinement might be deteriorated by this instability. This fact may not necessarily worsen the situation,

since, as will be shown later, the reduction of the energy confinement time can reduce the recharge time. At any rate, further experimental study on such a discharge with large electron drift velocity will be needed.

Other possibilities to reduce τ_r are the deterioration of the confine-confinement time and impurity contamination. Figure 10 shows the minimum recharge time τ_r and that for minimum P_s as a function of $\bar{n}_e$ when the energy confinement times of Eqs. (2.25) and (2.26) are halves i.e., $C_E = 0.5$. τ_r is reduced by a factor of 2 compared with the standard confinement scaling case of Fig. 5, since the electron temperature is reduced due to the deteriorated energy confinement.

Impurity contamination can also reduce τ_r. There are three major effects of impurity upon the recharge time τ_r. They are 1) decrease of current drive efficiency, 2) increase of the plasma resistivity, 3) increase of the radiation power loss. We reduce the current drive efficiency according to Fisch-Boozer's general expression [22],

$$\frac{j_{rf}}{P_{rf}} \propto \frac{6}{5 + Z_{eff}} \quad . \tag{3.1}$$

As for the radiation loss, we assume the oxygen impurity, and use Eq. (2.28).

Figure 11 shows the minimum recharge time as a function of $\bar{n}_e$ for various concentrations of oxygen impurity. τ_r is reduced by a factor of 1.6 for $f_z = 2\%$ compared with the case of $f_z = 0$. The increase of η dominates this reduction of τ_r, while the decrease of the current drive efficiency and the increase of joule heating due to the increase of η increase τ_r slighty. The effect of radiation loss is rather small, since the plasma density is very low.

From the above investigations we conclude that the essential point to reduce τ_r is driving sufficient current without increasing the plasma temperature too much. A possible difficult problem is, however, that the plasma, temperature of which is sustained only by the deposited rf power of Eq. (2.2), may be unstable for temperature perturbation. If the electron temperature is decreased by some perturbation, the number of resonant electron is reduced, so that the deposited rf power will also be reduced. Conversely, when the electron temperature is increased, the number of resonant electron is increased in the peripheral region of the plasma, so that all of the wave power is deposited there. As a result, the current profile may become hollow. In this case, however, the energy confinement may be deteriorated by the hollow profile, so that the electron temperature may be lowered again. At any rate, some control method will be required for the stable operation. For instance, if half of the heating power is supplied by other heating source than for current drive, e.g., electron cyclotron heating (ECH), the plasma will be far less unstable and could be controlled by adjusting ECH power. Figure 12 shows the minimum recharge time τ_r and that for minimum P_s as a function of $\bar{n}_e$ for this case. Since the electron temperature is high due to the additional heating power by ECH, the recharge time is increased by a factor of two than that in Fig. 5. Impurity contamination can reduce τ_r substantially as in the case of Fig. 11. It should be noted, however, that direct electron heating by LHW has not been taken into account so far. If this heating is substantial, this can play the same role as ECH and the plasma will be less unstable. This will be an important future study.

Although it is difficult to determine at present the definite parameters as an optimum, a rough range of the parameters to visualize the

reactor concept could be as follows.

$\bar{n}_e$: $(3 \sim 5) \times 10^{18}$ m^{-3}

$\bar{T}_e$: $3 \sim 5$ keV

τ_r : $3 \sim 5$ sec/V·s

P_{rf}: $8 \sim 16$ MW for current drive

n_z : $1.0 - 3.0 \sim 4.0$

2. Optimum plasma and rf parameters for Scenario II

Although almost all of the current drive experiments have been restricted to low density discharge, we assume that the current drive in higher density discharge (order of 10^{19} m^{-3}) will be achieved. This is a fundamental assumption for the Scenario II to be effective for the reactor. However, even when this restriction is removed, another restriction for the density due to the accessibility condition is expected. Thus, it is of primary importance to investigate the optimum plasma and rf parameters for maximizing Q value under the restriction of the accessibility condition.

Figure 13 shows the total driven current for various average electron density as a function of the upper parallel refractive index n_{z_1}. These currents are consistent with the power balance of the plasma as in the case of Scenario I. The lower parallel refractive index n_{z_2} is determined so as to satisfy the accessibility condition to the plasma center for each density, and is shown in the figure. When the spectrum is very narrow (n_{z_1} is close to n_{z_2}), the driven current is very small due to the small number of the resonant electron. The deposited power is also small, so that the temperature must be large to increase the α-heating power for the power balance, which leads to high Q value. As the width of

the spectrum is increased, the driven current increases very rapidly, while the temperature decreases as shown in Fig. 14 for $\bar{n} = 5 \times 10^{19}$ m^{-3} to keep the deposited power to the same level and reduce the α-particle heating for the power balance. Thus Q value gradually decreases. When the spectrum is further broadened, the decrease of the electron temperature determined by the power balance dominates, so that the driven current decreases. Consequently, the current takes its maximum at some n_{z1}. When the plasma density is high, α-particle heating tends to be more effective, so that the plasma temperature must be decreased for the power balance. The driven current should also be decreased due to the decrease both of the temperature and the spectrum width than the case with the lower plasma density.

There must be various restrictions on the magnitude of the driven current. Upper limit of the driven current should be determined by the safety factor at the plasma surface q_ψ. We set q_ψ to 2.5 to avoid the frequent plasma disruption. This value of q_ψ leads to $I_p = 5.3$ MA and is shown in Fig. 13 by long broken line. A possible lower limitation of the current may be the absolute confinement of α-particles, i.e. $I_p A \gtrsim 7.5$ [23]. The plasma current determined by this limitation is rather small and may be unimportant. More stringent restriction comes from the beta-poloidal limitation for the equilibrium and beta-toroidal limitation for the ballooning mode. We will use the following expression for the former limitation [24],

$$\beta_p \lesssim \frac{A}{2} \quad . \tag{3.2}$$

This restriction is denoted in Fig. 13 by oblique bar with β_p. We will not consider FCT equilibrium [25]. As for the latter restriction, we use the theoretical scaling for the available maximum beta value β_{max}^{theory} [26]

$$\beta_{max}^{theory} = 1.886 \times 10^{-1}\ q_{\psi}^{-0.54}\ (A - 1)^{-0.76} \quad , \tag{3.3}$$

where we have assumed κ (ellipticity) = 1.5 and omitted the small dependence on q_{ψ} of the exponent of κ. Considering the recent success of high beta experiments [27,28], we assume the same improvement factor as FER baseline parameter for the maximum available beta value β_{max} as

$$\beta_{max} \sim 1.5\ \beta_{max}^{theory} \quad . \tag{3.4}$$

The lower limit of I_p by this restriction is determined by the requirement that q_{ψ} should be greater than a certain value. This limitation is denoted in Fig. 13 by oblique bar with β_T. Usually maximum Q value is attained when the beta-poloidal limitation appears. They are shown in Fig. 15 with the fusion power as a function of the average electron density. In the figure, three cases for various energy confinement times are shown (i.e., $C_E = 1.0$, 0.75, 0.5). The case of $C_E = 1.0$ is the FER baseline case.

When the plasma density is low, the plasma temperature is increased to recover the α-particle heating. Thus, higher Q value is attained in lower plasma density, since the current drive efficiency is higher in lower plasma density with higher temperature. The increase of the plasma temperature dominates the decrease of the density, since $\langle\sigma v\rangle$ for D-T reaction begins to saturate in higher temperature, so that the plasma pressure is increased as the plasma density is lowered. Consequently, beta poloidal limitation cannot be satisfied within q_{ψ}-limitation for $\bar{n} \lesssim 4.5 \times 10^{19}$ m^{-3}. In this case, the maximum Q value is attained when q_{ψ}-limitation appears, (e.g., $Q \sim 1.0$ at $\bar{T}_e \sim 10$ keV, $n_{z1} \sim 1.83$ for $\bar{n} = 4.5 \times 10^{19}$ m^{-3}). Limitation of the Q value for each case is

dipicted by shaded boundaries. When the confinement is deteriorated ($C_E \sim 0.5$), α-particle heating must be effective, which leads to higher plasma density and fusion power. In all cases, the attainable Q value is $5 \sim 10$ and the fusion power is $300 \sim 500$ MW. These values agree with the results of a previous study [29]. One possible problem is that the required spectrum width is very narrow (1.51 - 1.57 for $\bar{n} = 5 \times 10^{19}$ m^{-3} and $C_E = 1.0$) and the dependence of the driven current on n_{z1} is very sharp, so that very careful spectrum and temperature control may be required to drive the desired current.

So far, we have not changed the device parameters from FER baseline parameters. However, in steady reactor, there is a possible advantage to remove all of the inner OH and equilibrium coils. In this case, the plasma major radius can be reduced. On the other hand, the toroidal magnetic field on axis is also reduced by the following scaling

$$B = B_{max}\left(1 - \frac{1 + \Delta/a}{A}\right) \quad , \tag{3.5}$$

where B_{max} and Δ are the maximum field at the inner surface of the coils and the distance between this surface and the inner surface of the plasma. We use $B_{max} = 12$ T and $\Delta = 1.4$ m in the following analysis. Figure 16 shows the maximum Q value and the fusion power for $\bar{n} = 4.5$ and 5×10^{19} m^{-3} as a function of the plasma major radius. The value of C_E is 1.0. Since the toroidal field in the plasma is reduced as in Eq.(3.5), the lower refractive index n_{z2} and also n_{z1} are increased by Eqs.(2.5) and (2.6). Then the plasma temperature must be decreased to keep the deposited rf power near the same level, so that the fusion power is decreased and Q value is also decreased as R is decreased. The possible minimum value of the major radius will be about 4 m from the structural restriction [30]. In this case, the maximum attainable Q value will

be 5 ∿ 7 for $\bar{n} = 4.5 \sim 5 \times 10^{19}$ m^{-3}. In the case of $\bar{n} = 4.5 \times 10^{19}$ m^{-3}, there appears β_p limitation on the plasma current for R > 4.5 m as in Fig. 13. Figure 17 shows the driven current and the deposited rf power for the case of Fig. 16. They vary only slightly with the major radius. Figure 18 shows the upper and lower parallel refractive index in the case of Fig. 16. The required width of the spectrum is very narrow for all cases. This will be a critical point for the design of the wave guide. Figure 19 shows the average electron and ion temperatures in the case of Fig. 16. The electron temperature is decreased as the major radius is decreased in accordance with the increase of the parallel refractive index in Fig. 18. When the electron temperature is increased, the ion temperature is further increased than the electron's due to the increase of the fraction of α-heating power partitioned to ions and also the increase of the electron-ion energy relaxation time. Figures 20 - 23 show the case with deteriorated confinement scaling ($C_E = 0.5$). Figure 20 shows the maximum Q value and fusion power for $\bar{n} = 7$ and 7.5×10^{19} m^{-3} as a function of the major radius. Figure 21 shows the driven current and deposited power. Figure 22 shows the upper and lower parallel refractive index. Figure 23 shows the average electron and ion temperatures. Qualitative feature of all the parameters are almost the same as those of the case with $C_E = 1.0$. However, required density for the power balance within beta limitation is higher i.e. $7 \sim 7.5 \times 10^{19}$ m^{-3}, since higher α-heating power is needed due to the deteriorated energy confinement. Required width of the wave spectrum is very narrow, so that the stringent control of the spectrum width and the driven current will be required as in the case of $C_E = 1.0$. If this control can be successfully achieved, maximum Q value of 5∿7 can be attained even if R = 4 m for $C_E = 1.0$ and 0.5.

4. Conclusions

Optimum plasma and rf parameters for possible operation scenarios by LHW current drive were studied by simple physical model equations. Two scenarios are considered as possible scenarios based on a present-day data base of the LHW current drive. The first is the quasi-steady operation, in which the current by LHW is driven only during the OH coil recharge phase with low plasma density. The second one is the steady operation, in which the plasma current is driven by LHW in burning phase with rather high density. The density restriction for the current drive in the present-day experiments must be removed for this scenario to be effective. The model equations are based on the quasi-linear theory of LHW current drive, a simple wave propagation, point model power balance and equivalent tokamak circuit.

In Scenario I, the essential parameter for the optimization is the recharge time τ_r or the required stored energy P_s. The key point to reduce τ_r or P_s is driving sufficient current without increasing the plasma temperature too much. In the case of standard FER baseline parameters, τ_r is shown to be $3 \sim 5$ sec/v.s. Deteriorated energy confinement and impurity contamination are shown to reduce τ_r and P_s substantially. Required spectrum width to realize the minimum τ_r and P_s is considerably wide. It is also shown that the plasma, temperature of which is sustained only by rf power for current drive, may be unstable for temperature perturbation, and some control method will be required.

In Scenario II, the essential parameter for the optimization is the energy multiplication factor Q. The key point to realize the highest Q value is appropriately adjusting the plasma density under the restriction of the accessibility condition, q_ψ limitation,

beta poloidal and toroidal limitations. The maximum attainable Q values for various energy confinement times and for various major radii are shown to be 5 ∿ 10. Required spectrum width is very narrow and the control of the driven current by this narrow spectrum is shown to be most critical.

We have not considered the detailed physical processes of the wave propagation, current drive and heating, since our primary purpose is to investigate the rough estimation of the optimum plasma and rf parameters for the conceptual design studies by a simple set of model equations. Although the feasibility and possible problems of both scenarios are roughly clarified in the present paper, more detailed discussions, especially on the spectrum modification due to the toroidal effect, reflection on the wall surface, direct electron heating, etc, are needed to determine the more definite optimum plasma and rf parameters. These will be our future plan for study.

Acknowledgements

The authors are grateful to Dr. M. Yoshikawa for useful suggestions and continuous encouragement throughout the work.

References

[1] Tomabechi T., Fujisawa N., Hiraoka T., Iida H., Naruse Y., et. al, in Plasma Physics and Controlled Nuclear Fusion Research (Proc. 9th Int. Conf. Boltimore, 1982) Vol. 1, IAEA, Vienna (1983) 399.

[2] Tone T., Fujisawa N., Seki Y., Iida H., Tachikawa K., et. al, to be published in Nuclear Technology/Fusion.

[3] Intor Group, "International Tokamak Reactor", Phase Zero, IAEA, Vienna (1980).

[4] Intor Group, "International Tokamak Reactor", Phase One, IAEA, Vienna (1982).

[5] Intor Group, "International Tokamak Reactor", Phase IIA, IAEA, Vienna (to be published).

[6] Fisch N.J., Phys. Rev. Lett. 41 (1978) 873.

[7] Karney C.F.F., Fisch N.J., Phys. Fluids 22 (1979) 1817.

[8] Yamamoto T., Imai T., Shimada M., Suzuki N., Maeno M., et. al, Phys. Pev. Lett. 45 (1980) 716.

[9] Hooke W., Sernabei S., Boyed D., Cavallo A., Chu T.K., in Plasma Physics and Controlled Nuclear Fusion Research (Proc. 9th Int. Conf. Baltimore, 1982) IAEA-CN-41/C-5.

[10] Tanaka S., Terumichi Y., Maekawa T., Cho T., Nakamura M., et. al, in Plasma Physics and Controlled Nuclear Fusion Research (Proc. 9th Int. Conf. Baltimore, 1982) IAEA-CN-41/C-1-3.

[11] Ohkubo K., Takamura S., Kawahata K., Tetsuka T., Matsuura K., et. al, Nuclear Fusion 22 (1982) 203.

[12] Ehst D.A., Nuclear Fusion 19 (1979) 1369.

[13] Yuen S.Y., Kaplan D., Cohn D.R., Nuclear Fusion 20 (1980) 159.

[14] White R.B., Monticello D.A., Rosenbluth M.N., Waddell B.V., in Plasma Physics and Controlled Nuclear Fusion Research (Proc. 6th

Int. Conf. Berchtesgaden, 1976) Vol. 1, IAEA, Vienna (1977) 569.

[15] Carreras B., Hicks H.R., Waddell B.V., Nuclear Fusion 19 (1979) 583.

[16] Porkolab M., Phys. Fluids 20 (1977) 2058.

[17] Porkolab M., Bernabei S., Hooke W.M., Motley R.W., Nagashima T., Phys. Rev. Lett. 38 (1977) 230.

[18] Clarke J.F., Nuclear Fusion 20 (1980) 563.

[19] Shimomura Y., JAERI-M 9065 (1980).

[20] Sugihara M., Fujisawa N., Ueda K., Saito S., Hatayama A., et. al, J. Nucl. Sci. Tech. 19 (1982) 628.

[21] Breton C., DeMichelis C., Mattioli M., Nuclear Fusion 16 (1976) 891.

[22] Fisch N.J., Boozer A.H., Phys. Rev. Lett. 45 (1980) 720.

[23] McAlees D.G., ORNL-TM-4661 (1974).

[24] Mukhovatov V.S., Shafranov V.D., Nuclear Fusion 11 (1971) 605.

[25] Clarke J.F., Sigmar D.J., Phys. Rev. Lett. 38 (1977) 70.

[26] Tuda T., Azumi M., Kurita G., Takizuka T., Takeda T., JAERI-M 82-104 (1982).

[27] Suzuki N., Imai T., Fujisawa N., Maeno M., Yamamoto T., et al, in Plasma Physics and Controlled Nuclear Fusion Research (Proc. 8th Int. Conf. Brussels, 1980) Vol. 2, IAEA, Vienna (1981) 525.

[28] Burrell K.H., Stambaugh R.D., Argel T.R., Armentrout C.J., Blau F.P., et. al, Nuclear Fusion 23 (1983) 536.

[29] Yoshizu T., Sugihara M., Fujisawa N., JAERI-M 82-165 (1982) (in Japanese).

[30] Sugihara M., Nishio S., JAERI-M 83-139 (1983) (in Japanese).

Table 1 Possible advantages for the reactor engineering by Scenario I and II. Size of the closed circle represents the degree of the advantage compared with the baseline FER. Cross represents no advantage.

Possible advantage	Major impact	Scenario I	Scenario II
1. Reduction of thermal and mechanical stress cycle	•Thermal stress of 1st wall •Mechanical stress of TF coil system	●	●
2. Increase of duty cycle	•Reactor relevancy	●	●
3. Possible reduction of disruption	•Life of 1st wall •Support system for e.m.f.	●	●
4. Reduction of peak power of PF coils in start-up phase	•Capacity of power supply	●	●
5. Reduction of stored energy, no. of energy transform	•Capacity of energy storage system •Energy loss during transform	●	●
6. Reduction of AC loss in supperconducting magnet in start-up/ shut-down phase	•Copacity of cooling system	●	●
7. Reduction of device size (major radius)	•Construction cost •Support system for e.m.f.	X	●

Table 2 Baseline device and plasma parameters of fusion experimental reactor (FER).

Plasma minor radius	a	(m)	1.1
Plasma major radius	R	(m)	5.5
Plasma elongation	κ		1.5
Plasma aspect ratio	A		5
Plasma current	I_p	(MA)	5.3
Safety factor	q_ψ		2.5
Field on axis	B	(T)	5.7
Average ion temperature	$\bar{T}_i$	(keV)	10
Average ion density	$\bar{n}_i$	(m^{-3})	1.4×10^{20}
Total fusion power	P_T	(MW)	440
Neutron wall loading	P_W	(MW/m^2)	1.0
Burn time		(sec)	100

Table 3 Circuit constants of equivalent circuit for the actual poloidal coils configuration of FER.

(H)

	Plasma	OH coil	V coil
Plasma	$13.5^{\times 10^{-6}}$	$155.1^{\times 10^{-6}}$	$1.222^{\times 10^{-3}}$
OH coil		0.494	0.281
V coil			2.2

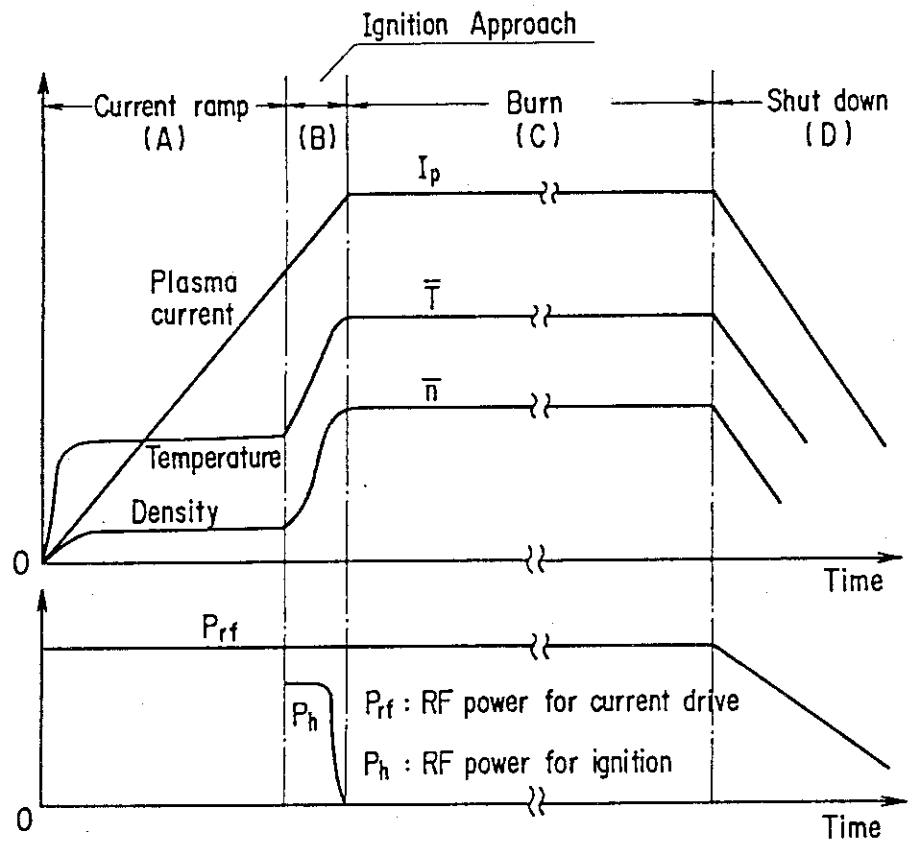

Fig. 1 A schematic drawing of steady operation scenario (Scenario II).

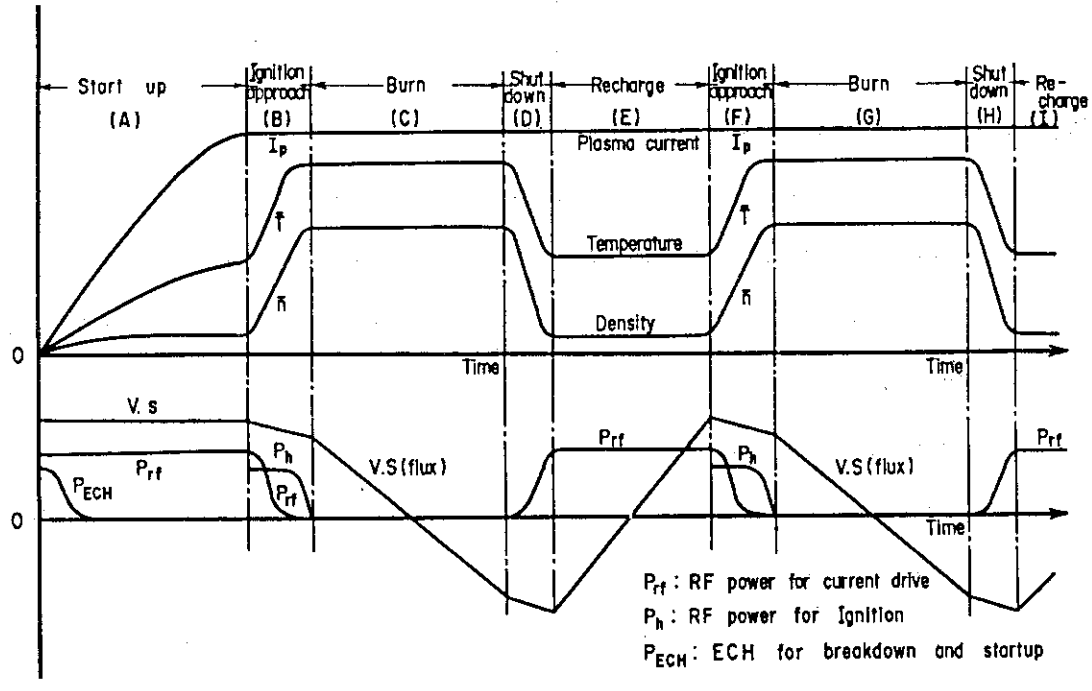

Fig. 2 A schematic drawing of quasi-steady operation scenario (Scenario I).

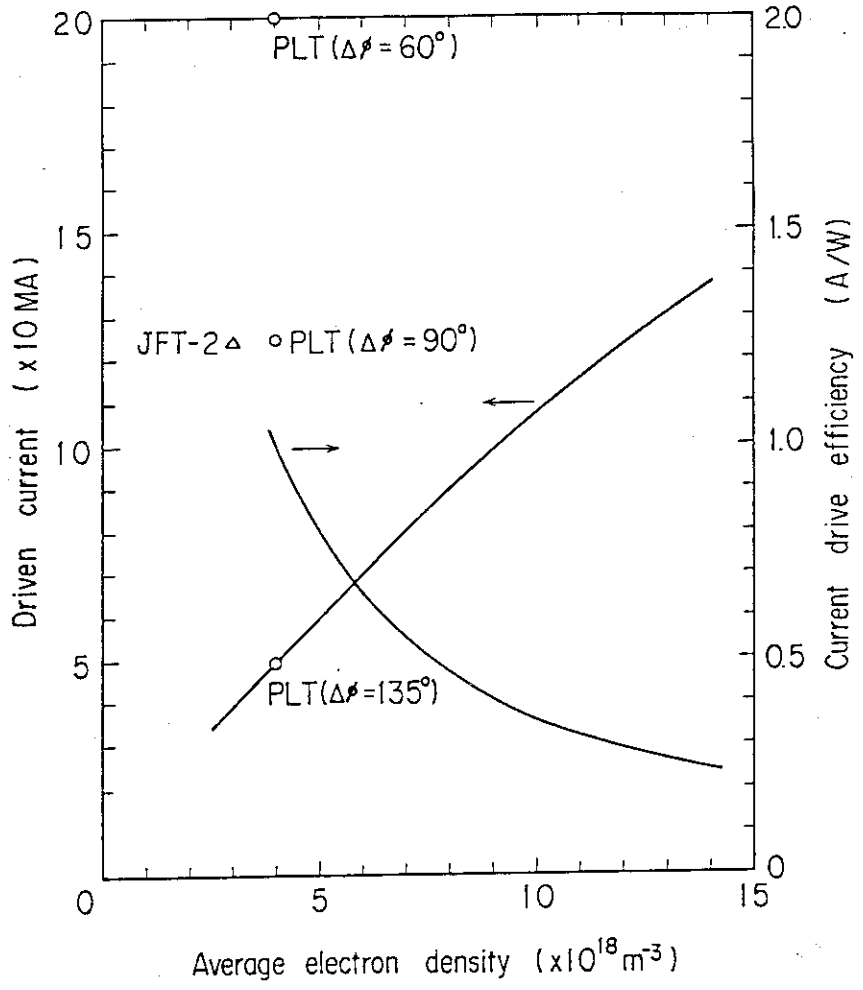

Fig. 3 Total driven current and drive efficiency for various average electron density. Average electron temperature is 1 keV. Upper parallel refractive index n_{z1} is 7.54, while lower refractive index n_{z2} is determined by the accessibility condition for each electron density. Intensity of wave spectrum is sufficiently strong, so that wave spectrum between n_{z1} and n_{z2} can penetrate to the plasma center. Open circles show the results of PLT experiment for various phase difference between the ajdacent wave guide. Open triangle shows the result of JFT-2 experiment extrapolated to the equivalent plasma with electron temperature of 1 keV.

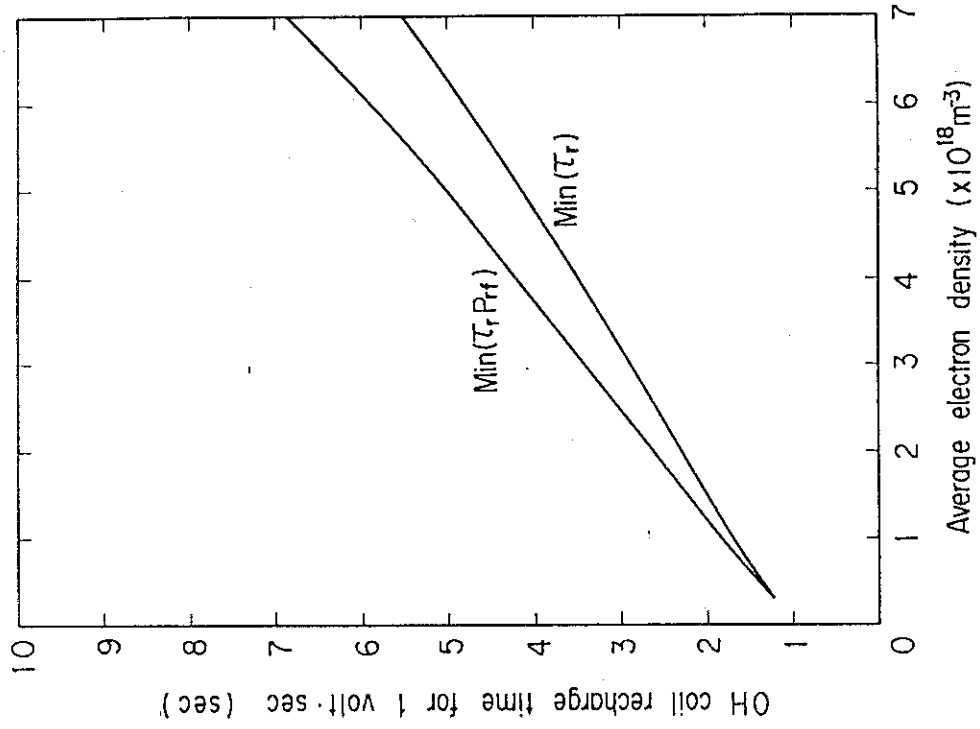

Fig. 5 Minimum recharge time of OH coils and that for minimum stored energy for 1 volt·sec as a function of the average electron density.

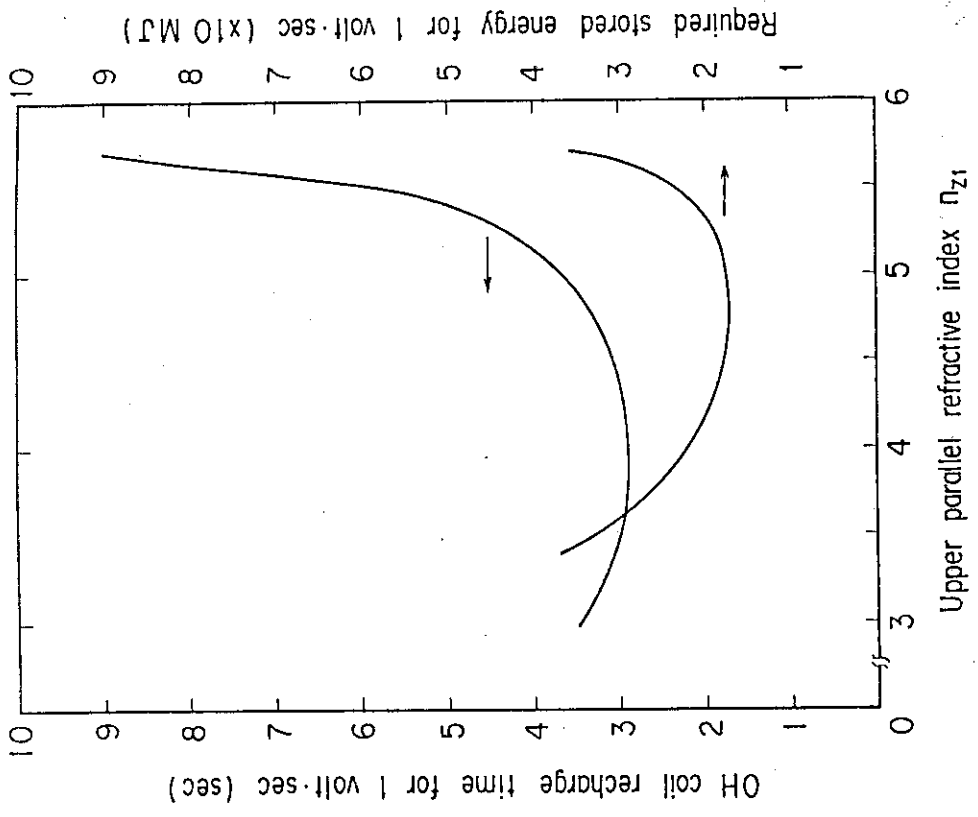

Fig.4 OH coil recharge time and required stored energy for 1 volt·second as a function of the upper parallel refractive index. Average plasma density is 3×10^{18} m^{-3} and $C_E = 1.0$ and no impurity contamination is assumed.

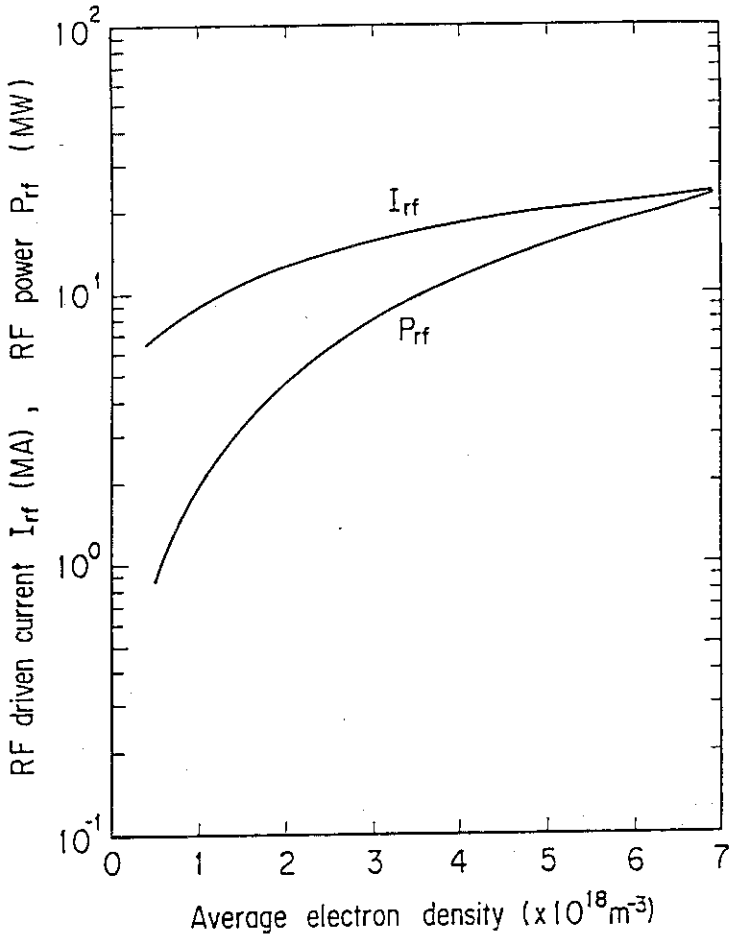

Fig. 6 Total driven current and deposited power for the minimum recharge time as a function of the average electron density.

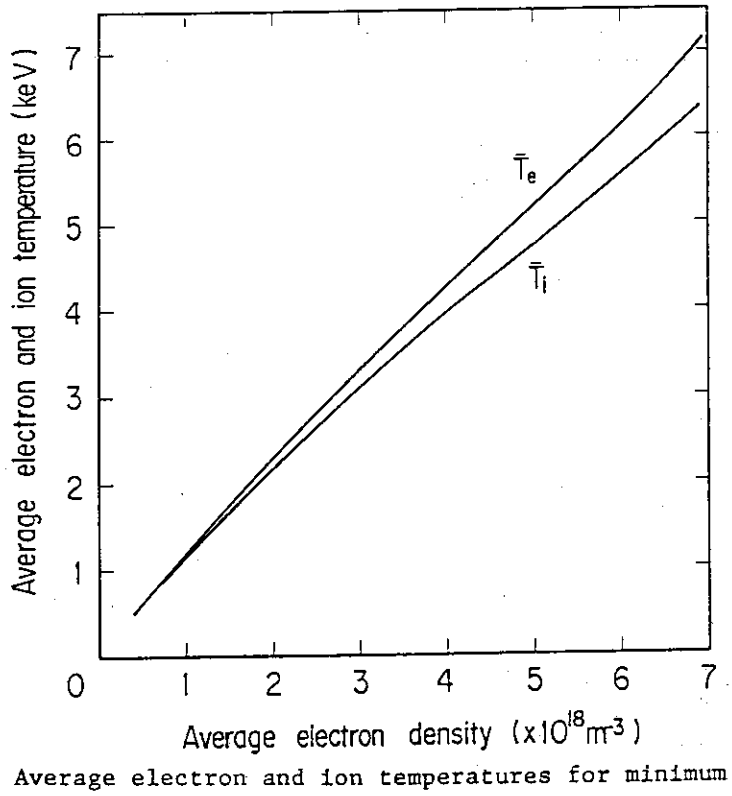

Fig. 7 Average electron and ion temperatures for minimum recharge time as a function of the average electron density.

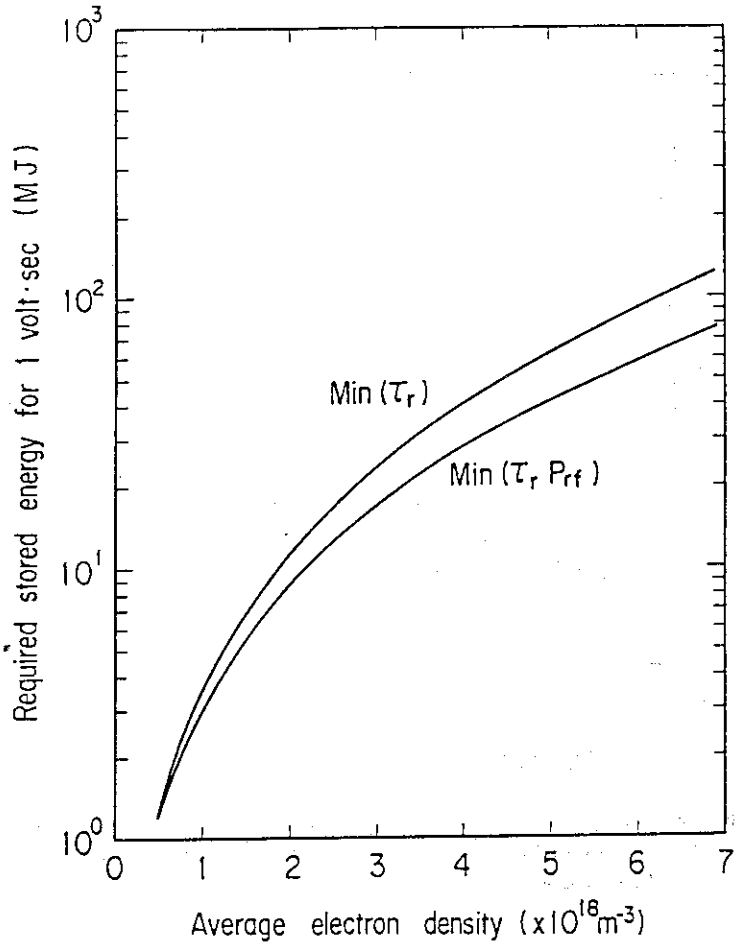

Fig.8 Minimum required stored energy and that for minimum recharge time for 1 volt·sec as a function of the average electron density.

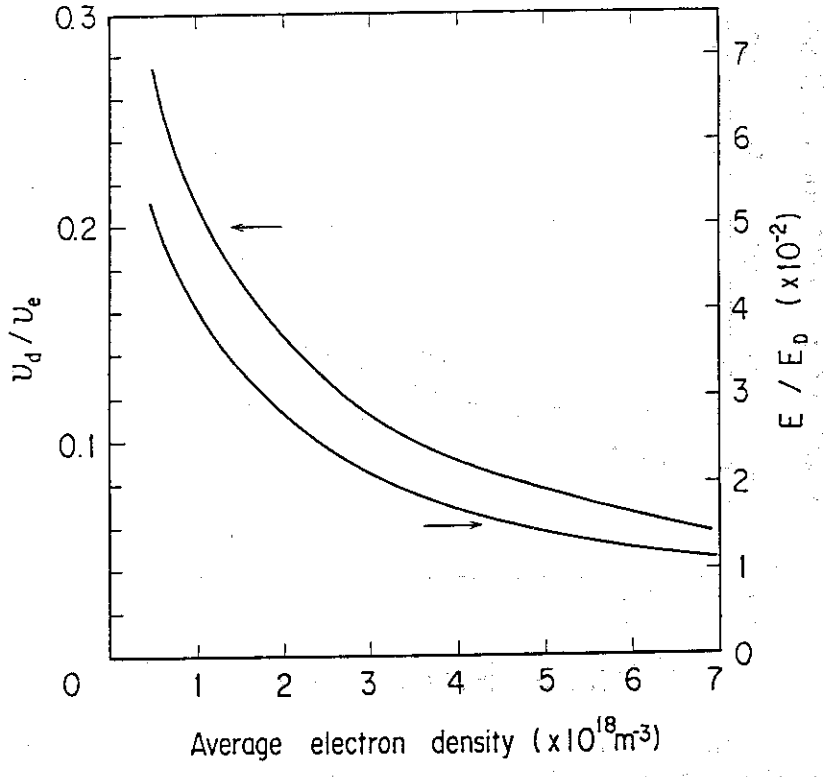

Fig.9 Ratio of the drift velocity to the thermal velocity of the bulk electrons and ratio of dc electric field by OH coils to the Dreicer electric field for the plasma parameters minimizing the recharge time as a function of the average electron density.

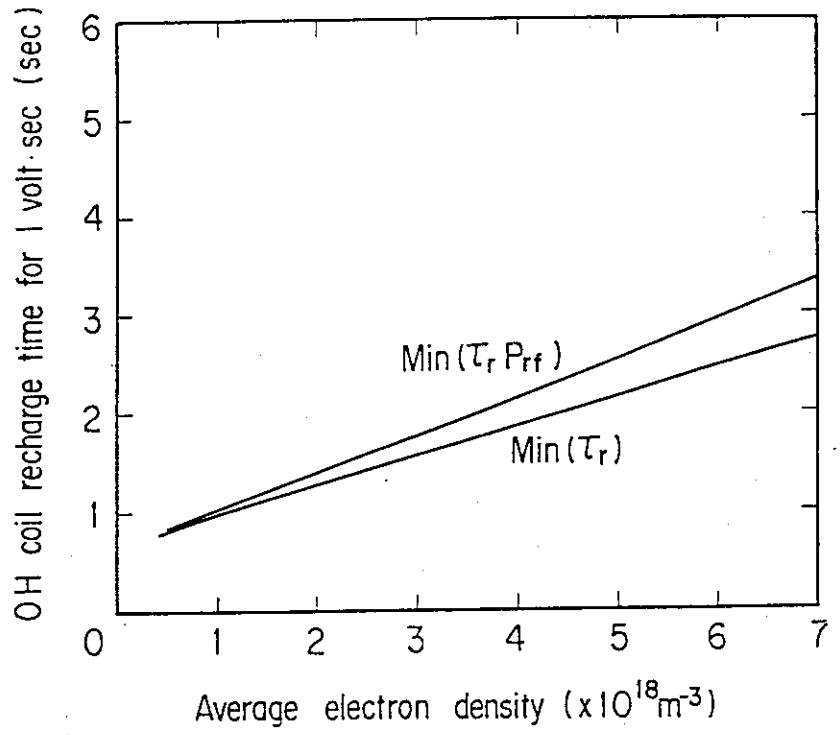

Fig.10 Minimum recharge time of OH coils and that for minimum stored energy of 1 volt.sec as a function of the average electron density in the case of the deteriorated energy confinement C_E=0.5.

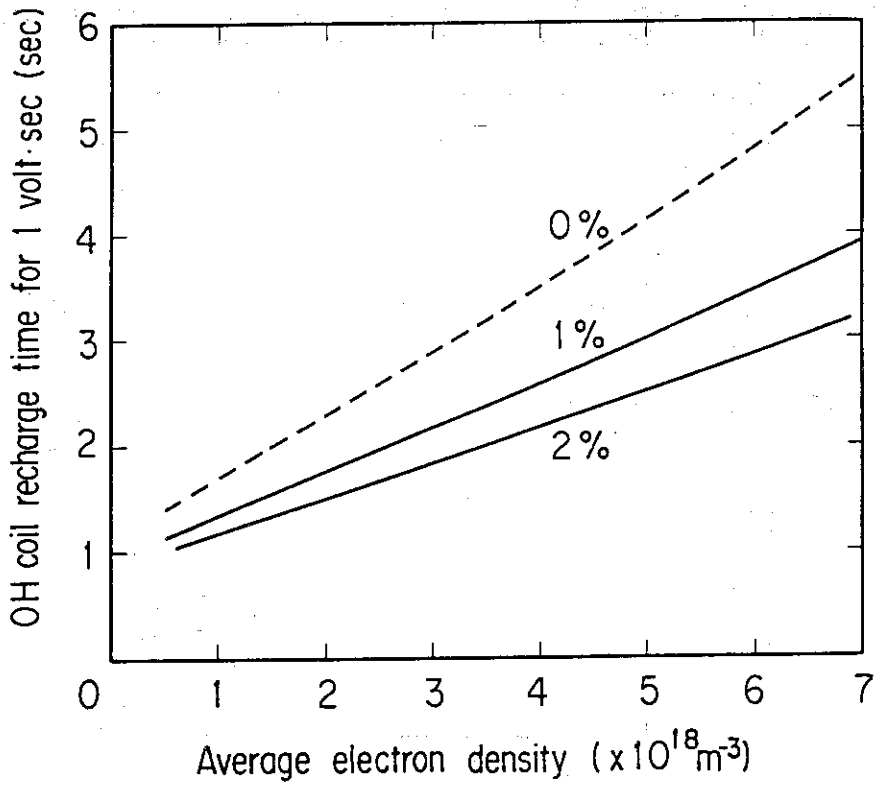

Fig.11 Minimum recharge time of OH coils for 1 volt·sec as a function of the average electron density in the case of oxygen impurity contamination. The case of no impurity contamination is also shown by dotted line.

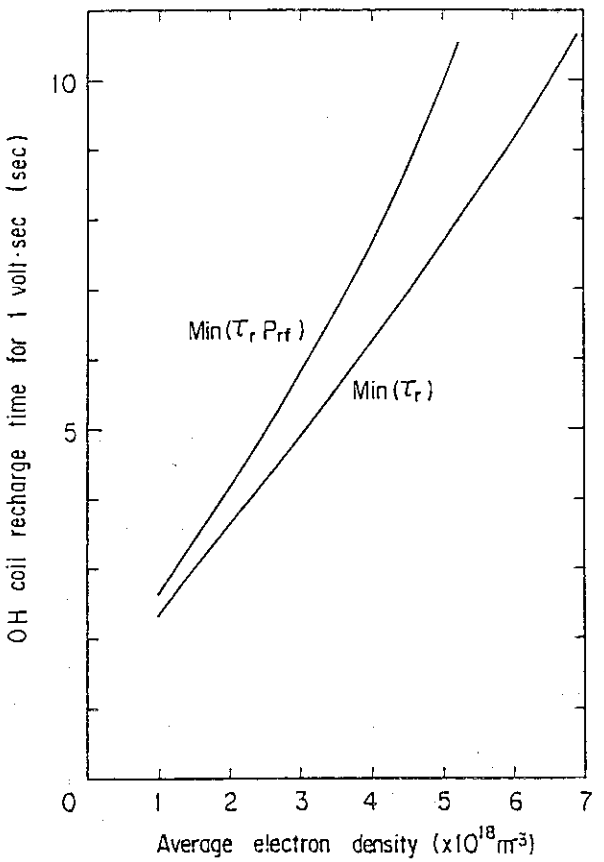

Fig. 12

Minimum recharge time of OH coils and that for minimum stored energy for 1 volt·sec as a function of the average electron density in the case of the additional ECH power to attain the stable operation. ECH power is assumed to be same as the deposited power for current drive. Impurity contamination is neglected and C_E = 1.0.

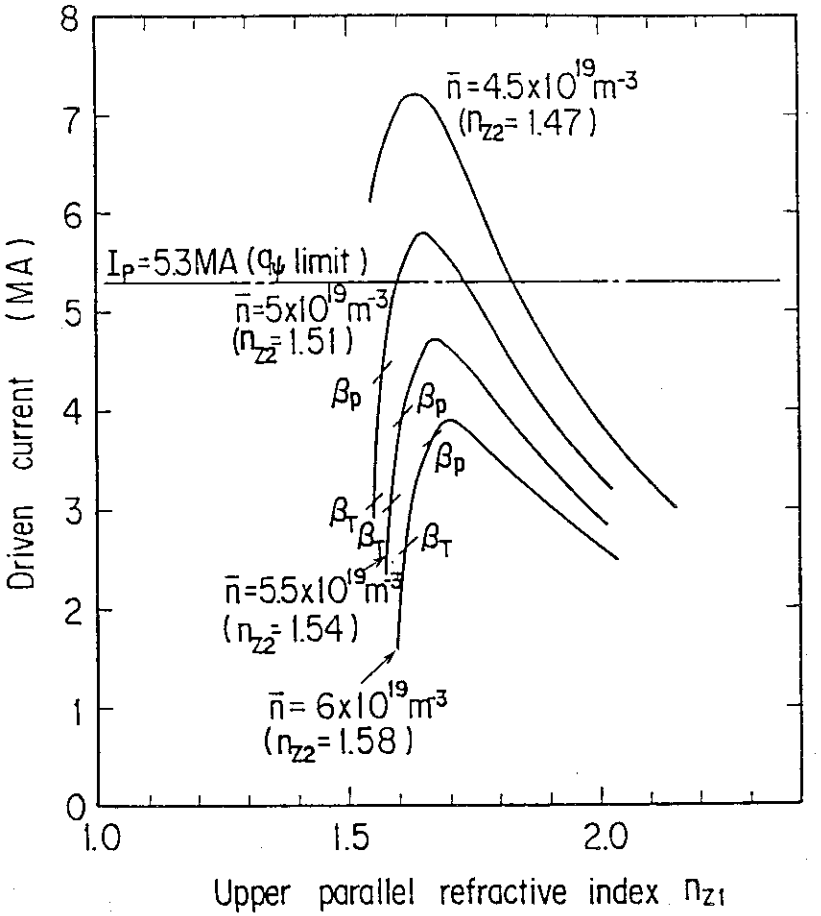

Fig. 13

Total driven current for various average electron density as a function of the upper parallel refractive index n_{z1}. The lower index n_{z2} is shown in the bracket for each density. The plasma current for q_ψ-limitation is shown by long dotted line. The plasma current for beta-poloidal and toroidal limitations are denoted by oblique bars with β_p or β_T.

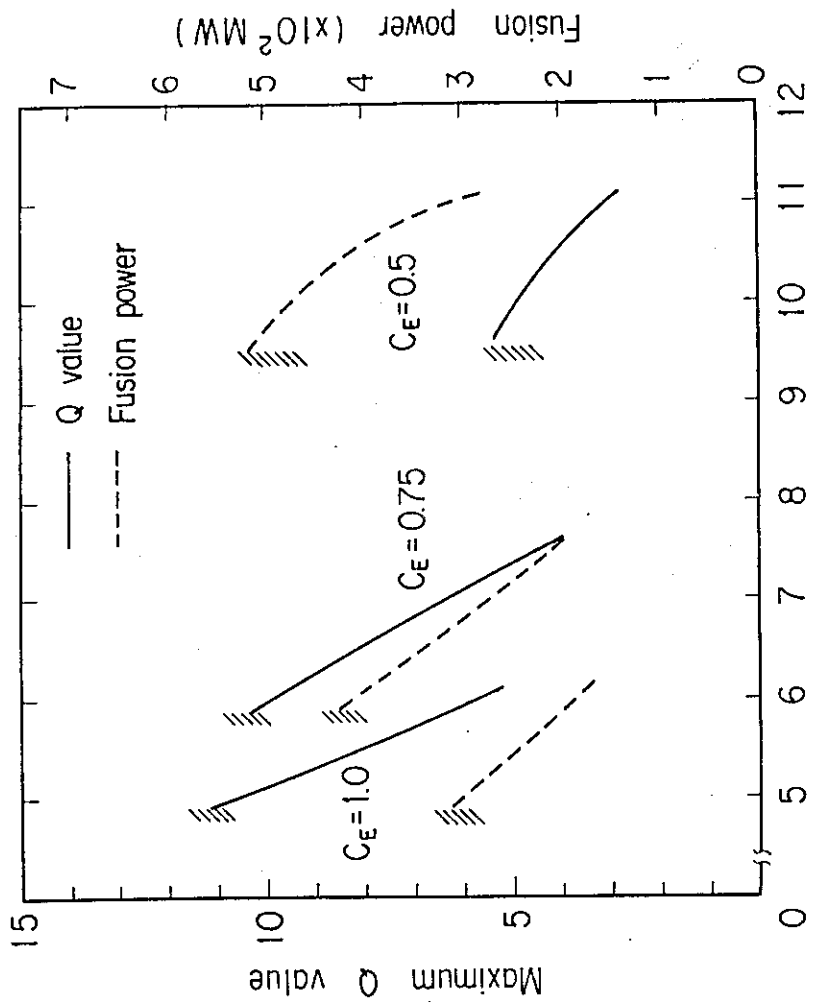

Fig. 15 Maximum attainable Q value and fusion power for various energy confinement times (C_E = 1.0, 0.75 and 0.5) as a function of the average electron density. Limitations for Q value are depicted by oblique lines.

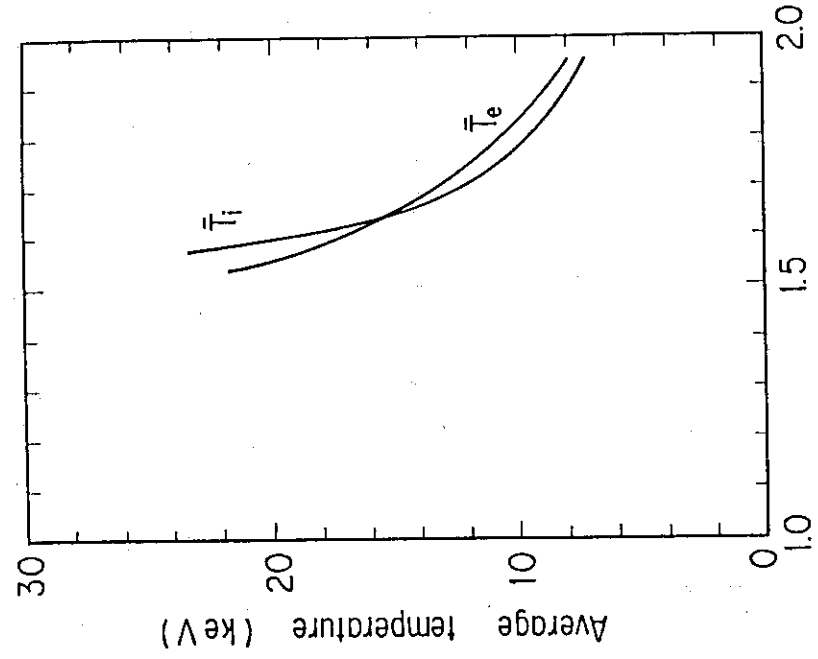

Fig.14 Average electron and ion temperatures as a function of the upper parallel refractive index n_{Z1} in the case of $\bar{n} = 5\times10^{19}m^{-3}$ of Fig.13.

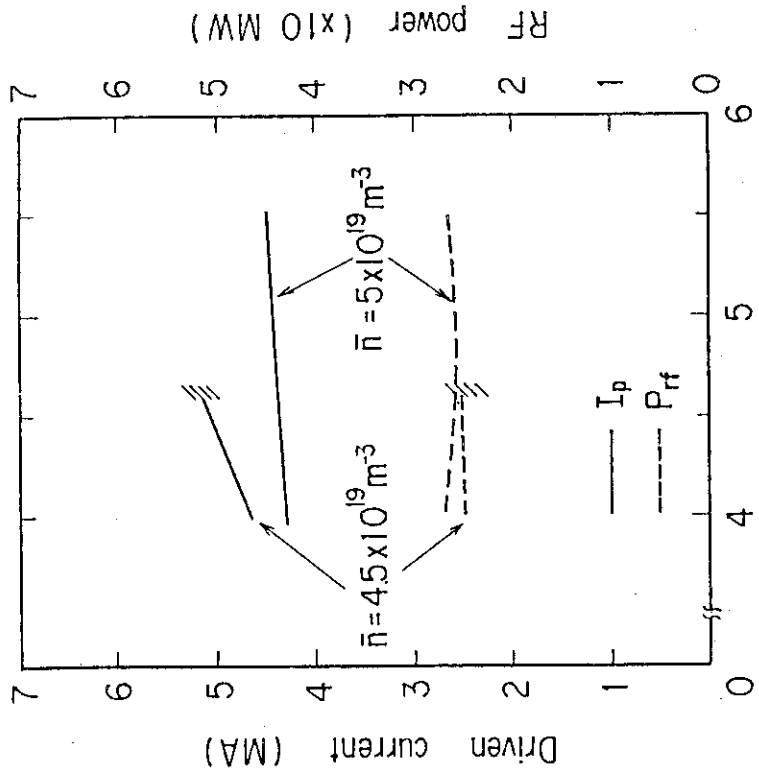

Fig.17 Total driven current and deposited rf power for the case of Fig.16 as a function of the plasma major radius.

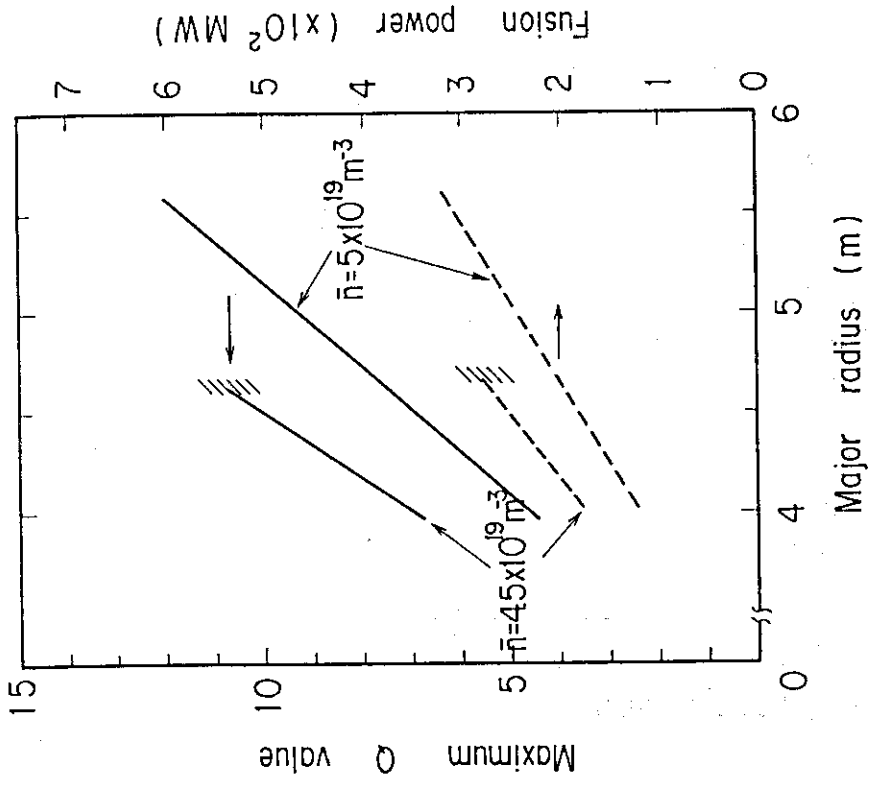

Fig. 16
Maximum attainable Q value and fusion power for $\bar{n}$ = 4.5 and 5×10^{19} m^{-3} as a function of the plasma major radius. B_{max} = 12T and C_E = 1.0. Limitation of Q value is depicted by oblique lines.

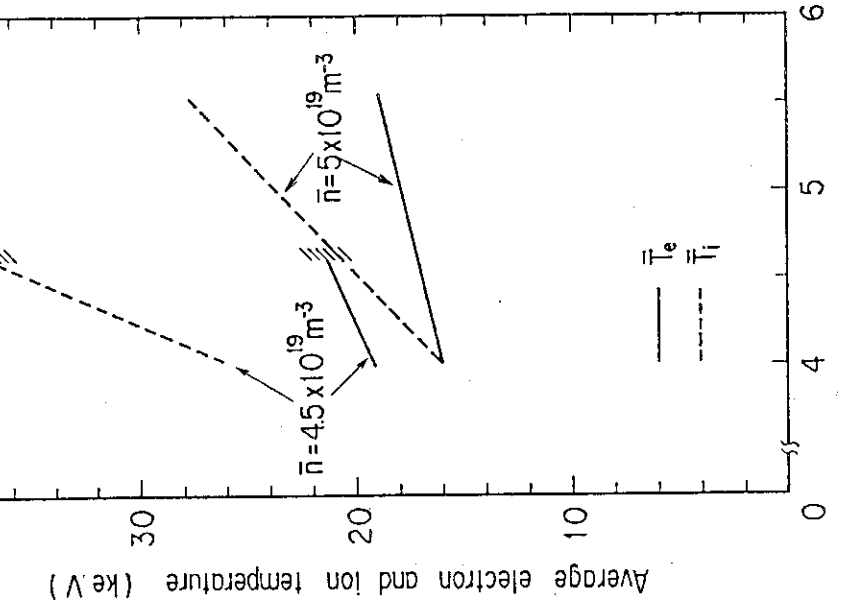

Fig.19 Average temperatures for the case of Fig.16 as a function of the plasma major radius. Solid line and dotted line show the average electron and ion temperature, respectively.

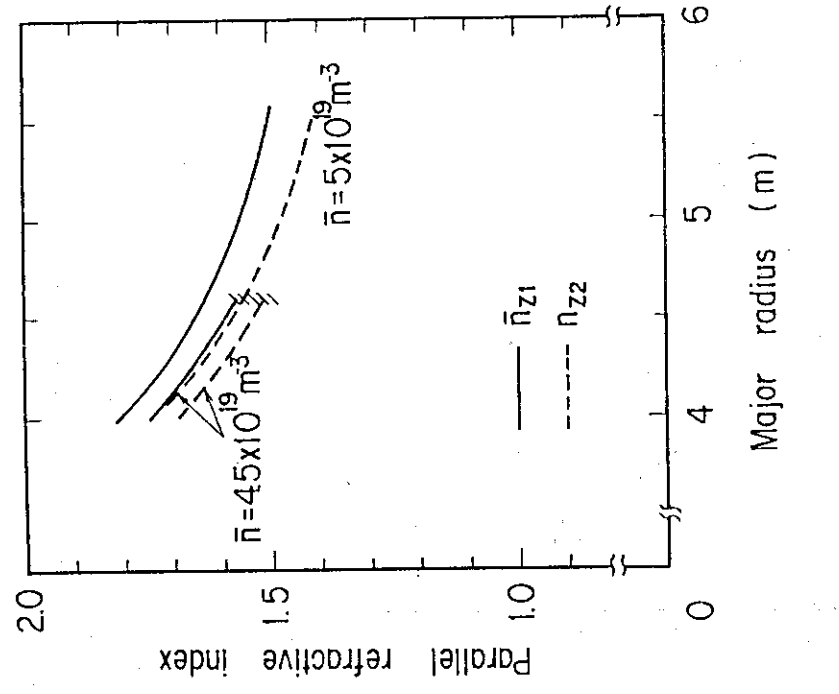

Fig.18 Parallel refractive index for the case of Fig.16 as a function of the plasma major radius. Solid line and dotted line show the upper and lower parallel refractive index, respectively.

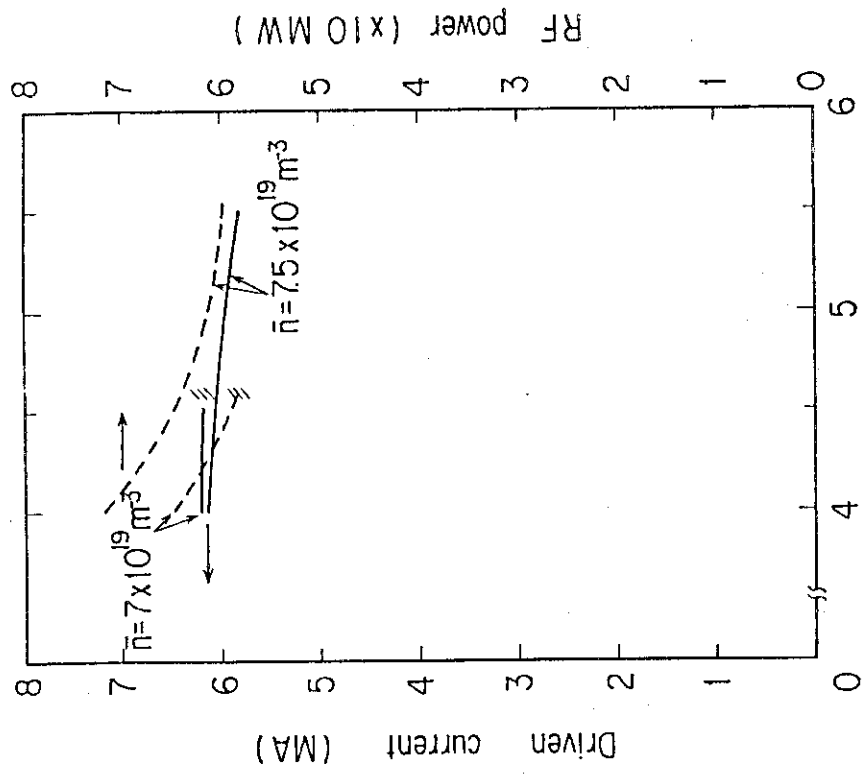

Fig.21 Total driven current and deposited rf power for the case of Fig.20 as a function of the plasma major radius.

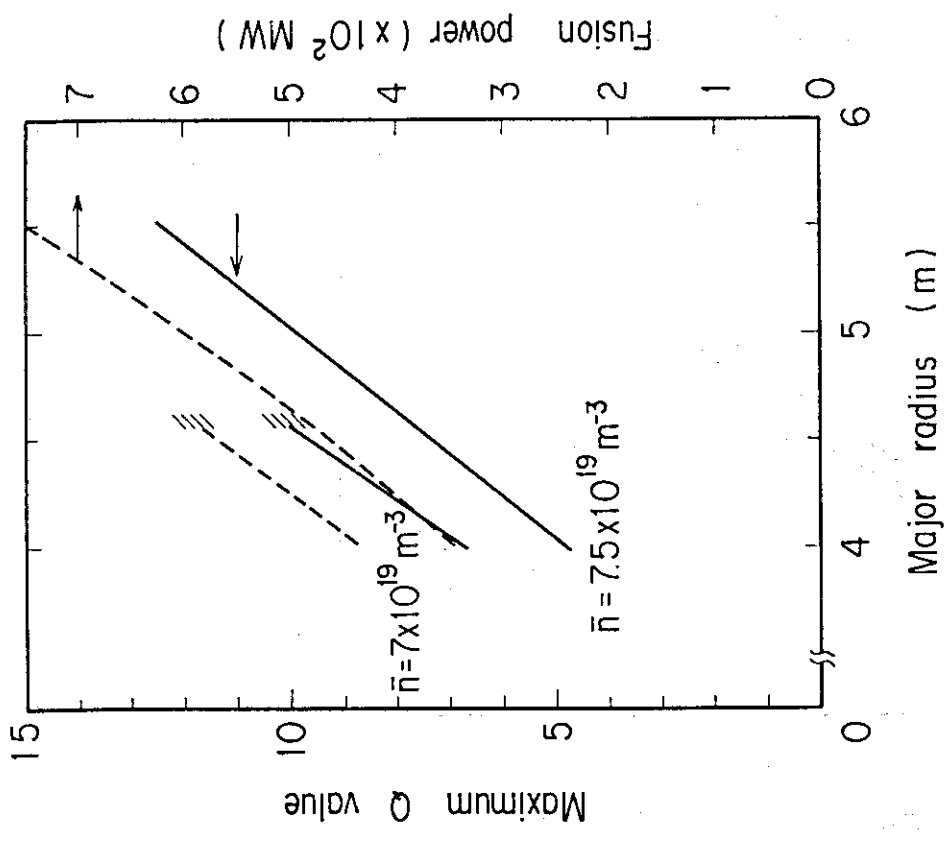

Fig. 20
Maximum attainable Q value and fusion power for $\bar{n}$ = 7 and 7.5×10^{19} m^{-3} as a function of the plasma major radius in the case of deteriorated energy confinement $C_E = 0.5$. $B_{max} = 12$ T. Limitation of Q value is depicted by oblique lines.

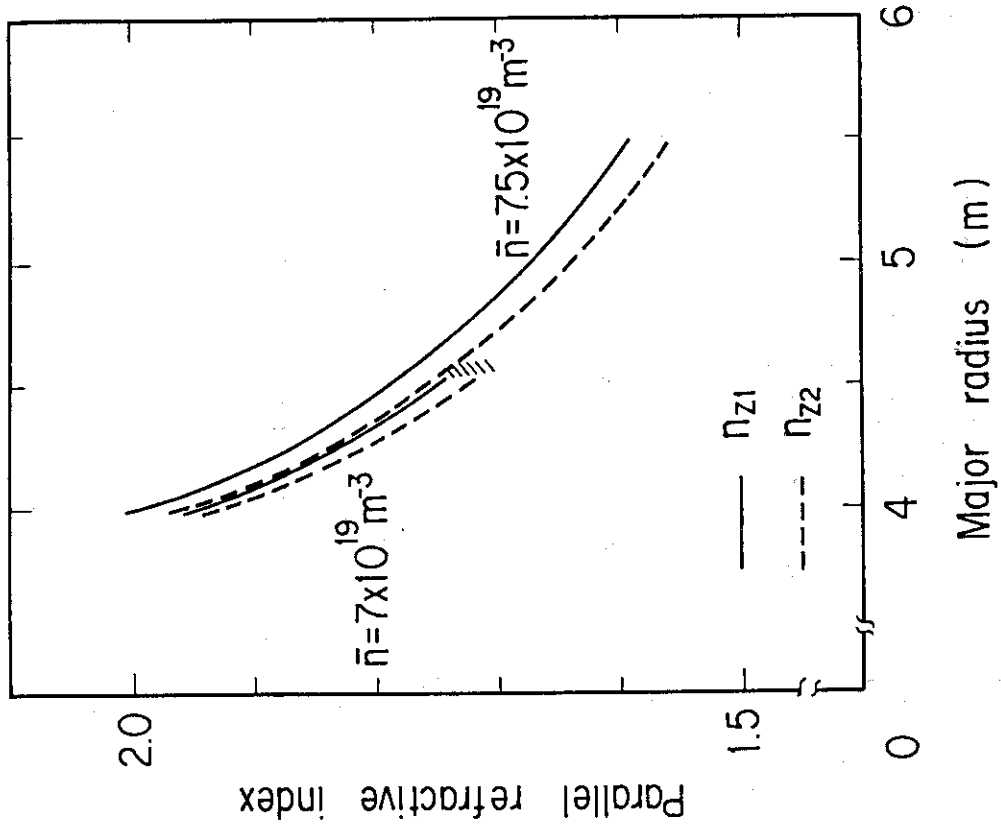

Fig.22 Parallel refractive index for the case of Fig.20 as a function of the plasma major radius. Solid line and dotted line show the upper and lower parallel refractive index, respectively.

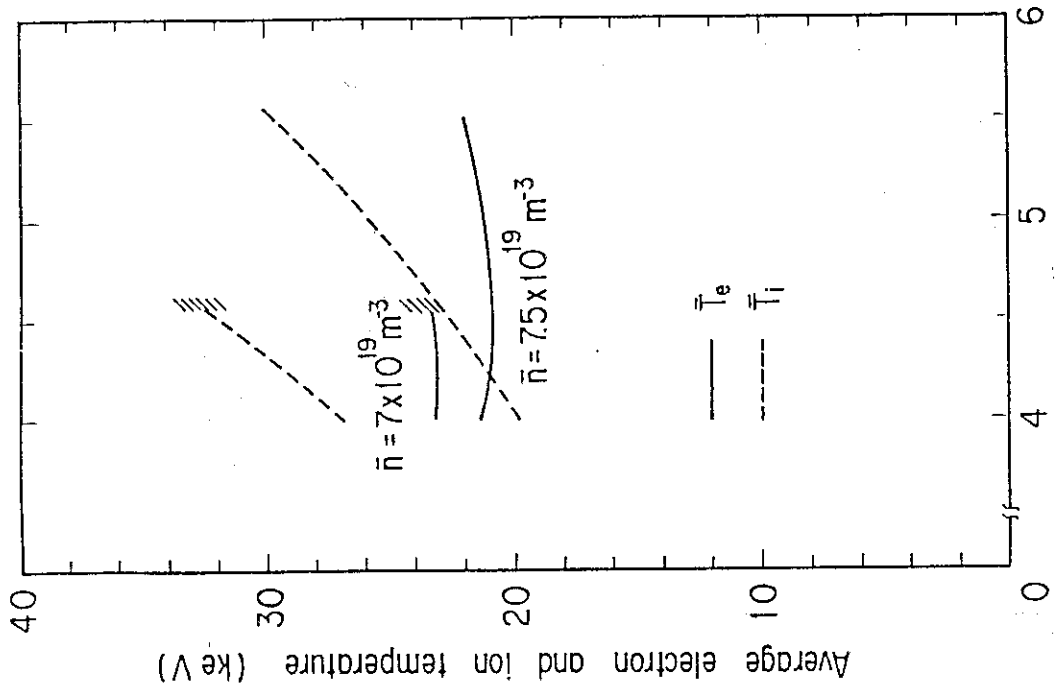

Fig.23 Average temperatures for the case of Fig.20 as a function of the plasma major redius. Solid line and dotted line show the average electron and ion temperature, respectively.